

PAPER

Width-dependent phase crossover in transition metal dichalcogenide nanoribbons

To cite this article: Wenyan Zan *et al* 2018 *Nanotechnology* **30** 075701

View the [article online](#) for updates and enhancements.

Recent citations

- [Progress and Prospects in Transition-Metal Dichalcogenide Research Beyond 2D](#)
Tomojit Chowdhury *et al*
- [Proximity-induced spin-orbit splitting in graphene nanoribbons on transition-metal dichalcogenides](#)
Yohanes S. Gani *et al*



IOP | ebooks™

Bringing together innovative digital publishing with leading authors from the global scientific community.

Start exploring the collection—download the first chapter of every title for free.

Width-dependent phase crossover in transition metal dichalcogenide nanoribbons

Wenyan Zan^{1,6} , Zhuhua Zhang² , Yang Yang³ , Xiaojun Yao⁴,
Sidian Li¹ and Boris I Yakobson^{3,5,6}

¹ Nanocluster Laboratory, Institute of Molecular Science, Shanxi University, Taiyuan 030006, People's Republic of China

² State Key Laboratory of Mechanics and Control of Mechanical Structures, Nanjing University of Aeronautics and Astronautics, Nanjing 210016, People's Republic of China

³ Department of Materials Science and NanoEngineering, Rice University, Houston, TX 77005, United States of America

⁴ State Key Laboratory of Applied Organic Chemistry, Department of Chemistry, Lanzhou University, Lanzhou 730000, People's Republic of China

⁵ Department of Chemistry and Smalley Institute for Nanoscale Science and Technology, Rice University, Houston, TX 77005, United States of America

E-mail: zanwy@sxu.edu.cn and biy@rice.edu

Received 16 August 2018, revised 9 November 2018

Accepted for publication 20 November 2018

Published 14 December 2018



Abstract

Two-dimensional (2D) transition metal dichalcogenides MX_2 ($\text{M} = \text{Mo}, \text{W}$; $\text{X} = \text{S}, \text{Se}$) exhibit two phases: the ground state 2H and the metastable 1T. Here, WSe_2 and MoS_2 monolayers have been studied, and we show by comprehensive first-principles calculations that the stability of the two phases can be switched in MX_2 nanoribbons. The 2H phase is found to have increasingly higher energy than the 1T phase at a smaller ribbon width, and the width for favoring the 1T phase reaches up to 2.50 nm for WSe_2 . The phase crossover is due to higher coordination of edge M atoms in 1T phase than in 2H phase and an interesting electronic reconstruction of 1T lattice in the ribbon interior. The edge configuration of 1T phase diminishes the edge dangling bonds and thereby enhances the stability of MX_2 nanoribbons. Our findings underscore the importance of edges in determining the structures of 2D MX_2 and are crucial for their future scientific studies and potential applications.

Supplementary material for this article is available [online](#)

Keywords: transition metal dichalcogenide, nanoribbon, first-principles calculations, phase crossover

(Some figures may appear in colour only in the online journal)

1. Introduction

Two-dimensional (2D) transition metal dichalcogenides (TMDs) MX_2 ($\text{M} = \text{Mo}, \text{W}$; $\text{X} = \text{S}, \text{Se}$), have attracted great research interest due to a number of exceptional properties and immense potential for applications in nanoelectronics and optoelectronics devices [1–8]. Being isomorphic to graphene and h-BN sheet, the MX_2 monolayers possess a honeycomb lattice, with the M atom sitting in one sublattice and the two X

atoms in the other. Yet, the 2D MX_2 is distinct in the metal-ligand bonding and the tri-atom thickness, with the M atoms sandwiched between two layers of X ligands. In particular, the two X layers can either be superimposed to form a trigonal prismatic phase, referred to as 2H- MX_2 , or be laterally shifted with respect to each other to form an octahedral phase, referred to as 1T- MX_2 [9–13]. The 2D 2H- MX_2 is considerably, by 0.50–0.9 eV per primitive cell, lower in energy than the 1T- MX_2 , depending on M and X atoms [14]. What is more, the 2H- MX_2 is a 2D semiconductor with a direct band gap of 1.1–2.1 eV while the 1T- MX_2 is metallic with high

⁶ Authors to whom any correspondence should be addressed.

surface reactivity [15–17]. Such contrasting electronic property raises the possibility of fabricating in-plane metal–semiconductor junctions with atomically smooth interfaces and coherent atomic compositions.

While the 2D forms of TMDs offer great promise, real applications in using these materials require only a small piece of them, instead of an infinite size. Moreover, for the development of current electronic technology, the individual elements of devices should continue to shrink to meet the increasing demand of enhanced performance. Thus, it is of technological importance to explore the 1D ribbons of nanometer scale with well-defined edges. Compared with the extensively studied 2D TMDs [18–22], the 1D nanoribbons, however, have not received due attention. Fabrication of MX_2 nanoribbons and wires has been implemented in experiments [23–25]. Theoretically, it is reported that the MX_2 nanoribbons exhibit unusual electronic and magnetic properties, including edge magnetism and orientation-dependent transport behaviors [26–28]. Nevertheless, all the theoretical proposed structures of nanoribbons are simply cut from the 2H- MX_2 monolayer. Such adoption of ribbon structures seems arbitrary in a sense that the ground state structure of 2D MX_2 is quite vulnerable to various imperfections, such as charge doping, adsorption of metal atoms, electron irradiation and application of the strain [29–33]. It is natural to anticipate that the presence of edges may alter the structure of MX_2 nanoribbon in unusual ways [8, 34]. Despite the extensive study of nanoribbons of graphene and h-BN, little can be generalized to the MX_2 family, where qualitatively new phenomena can be found.

Here, we show, by first-principles calculations, that the MX_2 nanoribbons undergo a spontaneous phase transition from 2H to 1T, at least for those with zigzag and armchair edges, a behavior rarely seen in other types of 2D materials. We find that the transition becomes more energetically favorable with decreasing ribbon width or increasing the atomic radii of M and X. The critical ribbon width favoring the 1T phase reaches up to 2.50 nm for the 2D WSe_2 . The origin of the phase transition is related to effective edge self-passivation enabled by the 1T phase.

2. Theoretical methods

The density functional theory calculations were carried out by using Vienna *Ab initio* simulation package code [35]. The projector augmented wave method [36] for potentials at the core region and spin-polarized DFT based on the generalized gradient approximation of PBE functional were adopted [37]. A kinetic energy cut-off of 400 eV was used for the plane-wave expansion. The k-point grids in the first Brillouin zone of armchair and zigzag ribbons were $4 \times 1 \times 1$ and $8 \times 1 \times 1$. All atomic positions were fully relaxed using the conjugate-gradient method until the force on each atom was less than $0.01 \text{ eV } \text{\AA}^{-1}$.

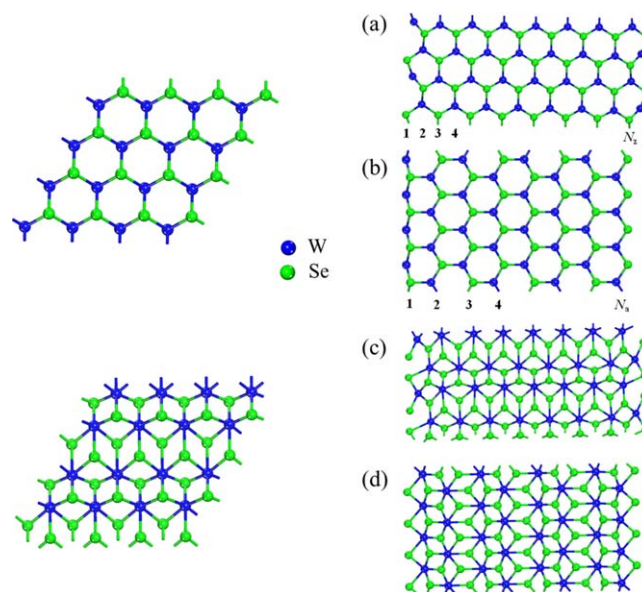


Figure 1. The most stable configurations of (a) 2H-16-aWNR, (b) 2H-8-zWNR, (c) 1T-16-aWNR and (d) 1T-8-zWNR. Blue and green spheres stand for the W and Se, respectively.

3. Results and discussion

3.1. Geometric structures and formation energies

The initial MX_2 nanoribbons can be directly obtained by shaping the 2H MX_2 monolayers along specific crystallographic orientations. According to the edge orientation, two typical types of nanoribbons can be obtained: armchair and zigzag. In contrast to graphene and h-BN with only one overwhelmingly stable lattice structure, the MX_2 monolayer has two polymorphs: 2H and 1T phases. The MX_2 nanoribbons in 1T phase are also considered. Since most MX_2 monolayers have the same lattice structures and show very similar electronic behaviors, we mainly focus our discussion on WSe_2 , which is used as a prototype model system. The nanoribbons of other 2D materials in this family will be discussed later. Following the convention, we use N_z and N_a to characterize the width of zigzag and armchair nanoribbons, where N_z and N_a are the number of zigzag lines and dimer lines across the ribbon width, respectively. For ease of discussion, we use notation N_a -aWNR to describe an armchair WSe_2 nanoribbon with N_a dimer lines and N_z -zWNR to describe a zigzag WSe_2 nanoribbon having N_z zigzag lines. Figure 1 presents the optimized geometries of 2H and 1T 8-zWNR and 16-aWNR. After full relaxation, the interior lattices (triple-layer networks) are well kept for all the 2H and 1T nanoribbons. For the 2H nanoribbons, structural distortion takes place along the edges, mostly around the W atoms (they tend to shift inward slightly), which have less coordination than those in the perfect lattice. This distortion appears to be severer along the W edges of zWNR than along those in the aWNR. In contrast, the edge distortion becomes less evident along the edges of 1T nanoribbons. This observation raises an interesting question regarding whether the edge of 1T phase is more favorable than that of 2H and therefore motivates us to

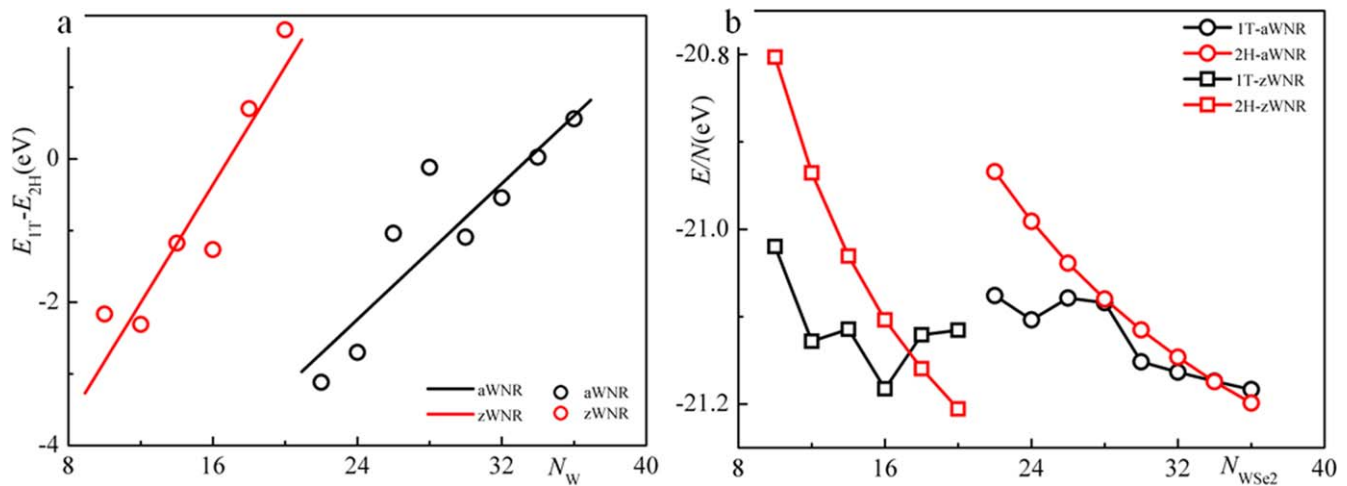


Figure 2. (a) The energy differences between 1T/2H-WNRs as a function of the number of the W atoms, (b) the energy per formula unit of 1T/2H-WNRs as a function of the number of formula units. The lines are the fitting results, and the dots are data points.

examine the relative stability of nanoribbons with different phases.

We then compare the stability of 2H and 1T phases for a series of nanoribbons, in 2H and 1T phases yet with the same stoichiometry. The energy differences between 1T and 2H WSe₂ nanoribbons per supercell as a function of ribbon width are displayed in figure 2(a). For large-scale aWNR, the 2H phase is more favorable than the 1T phase, following the same order as in perfect 2D lattice. Yet, the energy difference between the 2H and 1T phases sharply decreases with decreasing ribbon width, and, surprisingly, the 1T phase becomes more stable than the 2H phase when the ribbon width is smaller or equal to 2.50 nm (i.e. critical width, see figure 2(a)), indicating that thermodynamically, the 1T phase becomes the ground state. Similar results also occur in the zWNR, whose critical width is 2.08 nm. The switch of relative stability is further confirmed in figure 2(b), where the energy normalized by the number of W atoms (N_W) in the nanoribbons is shown as a function of N_W . For 1T WNRs, the non-monotonic behavior of the energy versus ribbon width is attributed to their structural distortion displaying as the moving of every other metal chain along the ribbon closer to one neighbor and further away from the other. While the normalized energy increases with decreasing N_W for both types of ribbons, the curve for 2H WNRs increases more sharply than that for the 1T WNRs. Since the WNRs with a smaller N_W have a higher ratio of edge atom, this result suggests that the edge energy of 2H WNRs is higher than the 1T WNRs, resulting in the higher stability of 1T nanoribbons when N_W is below certain value. Additional calculations show that the size-dependent phase crossover of MX₂ nanoribbons is robust against interaction from commonly used substrates, such as Cu and SiO₂ substrates (see figures S1 and S2, available online at stacks.iop.org/NANO/30/075701/mmedia).

The MoS₂ nanoribbons show similar behavior and have smaller critical widths, which are 1.45 and 1.47 nm for aMoNR and zMoNR, respectively (see figure S3). The trend results from the fact that the energy difference between 2H

phase and 1T phase is higher in MoS₂ (0.85 eV) than in WSe₂ (0.75 eV).

Our above results have shown that the energy difference, ΔE , between the 1T and 2H nanoribbons closely relies on the nanoribbon width. To gain further insight, it would be useful to constitute an analytical relationship between ΔE_{1T-2H} and ribbon width. Starting from the 1T and 2H nanoribbons, we could write their total energy, E_{rib} , in two contributions: the edge energy per unit length (here the unit length is the lattice constant of the corresponding MX₂ monolayer) γ and the energy of interior perfect lattice E_{int} . Note that γ is a constant while E_{int} is proportional to the number of M atoms, N_M , in the unit cell of a ribbon, which equals N_a for aMNRs and N_z for zMNRs. In this way, the total energy of the ribbons can be expressed as

$$E_{rib} = \gamma L + E_{MX_2} N_M, \quad (1)$$

where E_{MX_2} is the energy per MX₂ unit of a perfect 2H MX₂ monolayer for 2H nanoribbons and that of a perfect 1T MX₂ monolayer for 1T nanoribbons. L is the length of 2H and 1T nanoribbons.

For the total edge energy of a ribbon, γ can be calculated as $\gamma L = E_{rib} - E_{MX_2} N_M$. By calculating γ and E_{MX_2} , we obtained $\Delta E_{1T-2H} = -6.90 + 0.41N_z$ for the zWNRs, and $-7.88 + 0.24N_a$ for the aWNRs. Likewise, $\Delta E_{1T-2H} = -8.16 + 0.65N_z$ for zMoNRs and $-12.26 + 0.57N_a$ for aMoNRs. The analytical results of ΔE_{1T-2H} for the WNRs are shown by solid lines in figure 2(a), showing excellent agreement with direct DFT calculations. These analyses further reveal that the enhanced edge stability of 1T phase is the major driving force for the phase crossover in narrow nanoribbons.

We have noted that the preceding 2H and 1T MX₂ nanoribbons have the same stoichiometry. Yet, in reality the edges of nanoribbons may have varied passivations, manifested as different converges of X along the edges. In particular, the bare zigzag Mo edge of 2H phase is likely to be passivated by additional S atoms. To examine the effect of edge passivation, we consider a 50% coverage of sulfur at

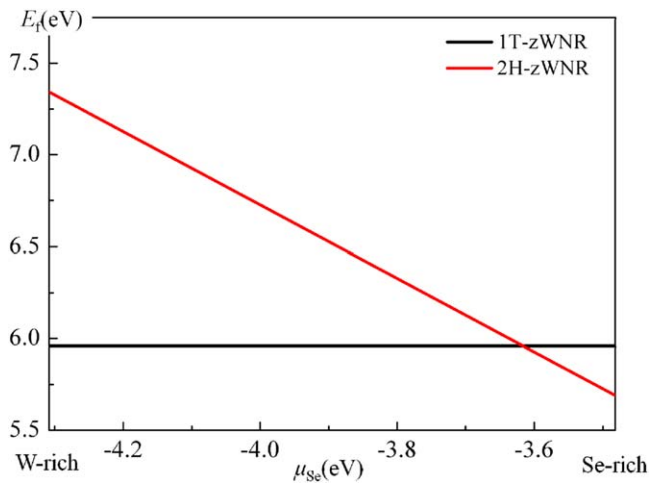


Figure 3. Formation energies of 2H/1T-5-zWNR as a function of Se chemical potential, plotted in the range $-4.31 \text{ eV} < \mu_{\text{Se}} < -3.48 \text{ eV}$, where WSe_2 can be thermodynamically favorable with respect to the formation of bulk W ($\mu_{\text{Se}} = -4.31 \text{ eV}$) or Se crystal ($\mu_{\text{Se}} = -3.48 \text{ eV}$).

the Mo edge of a 2H-5-zWNR, then the edge modified 2H-5-zWNR is compared to a 1T-5-zWNR without edge modification. Relative stability of the two nanoribbons with different stoichiometry can be compared by calculating the formation energy E_f , defined as

$$E_f = E - N_W E_{\text{WSe}_2} - N_{\text{Se}} \mu_{\text{Se}}, \quad (2)$$

where E is the total energy of the nanoribbons, E_{WSe_2} is the energy per WSe_2 unit in perfect 2H monolayer, N_W is the number of W atoms in the nanoribbons, N_{Se} is the number of extra Se atoms in the nanoribbon with respect to that in the nanoribbon without edge modification (i.e. $N_W:N_{\text{Se}} = 1:2$) and μ_{Se} is the chemical potential of Se. Apparently, the relative stability between the 1T-5-zWNR and edge modified 2H-5-zWNR depends on μ_{Se} (see figure 3). Under Se-deficient condition, the 1T-5-zWNR remains more stable than the edge modified 2H-5-zWNR until μ_{Se} is increased to -3.62 eV , above which the edge modified 2H-5-zWNR become increasingly more favorable. These results suggest that a phase crossover in MX_2 nanoribbons may be facilitated by reducing the chemical potential of X during CVD synthesis.

3.2. Densities of states and band structures

To get further insight into the phase switch of WSe_2 and MoS_2 nanoribbons, we examine electronic structures of the nanoribbons with different phases and sizes. As is known, 1T phase is distinctly less stable than the 2H phase for perfect 2D MX_2 lattice. This difference in stability is reflected in their electronic structures, especially the density of states (DOS) near the Fermi level. The 2H MX_2 monolayer has zero DOS in a certain energy window near the Fermi level; whereas the 1T monolayer shows rich electronic states across the Fermi level, which are high in energy and therefore degrade the system stability. In contrast to 2D monolayer, their nanoribbons are made of edges and perfect lattice in the interior. The edges introduce dangling bonds that manifest as

additional high-energy electronic states around the Fermi level. So the competition of stability between the edge and interior lattice may give rise to variability of lattice phase in the nanoribbons.

Figure 4 presents the mapping of spatially resolved local DOS across the 1T and 2H-14, 18-aWNR. For the N_a -aWNR, the site-dependent local DOSs from the edge to the center are obtained by averaging the DOSs of n th and $(N_a + 1 - n)$ th dimer lines (in mirror symmetry with respect to the ribbon center), while that for the N_z -zWNR are obtained by averaging the DOSs of W in the n th zigzag chain and Se in the $(N_a + 1 - n)$ th chain (or Se in the n th zigzag chain and W in the $(N_a + 1 - n)$ th chain if the Se is in position from the left). For the 2H-18-aWNR, the DOSs contributed by the interior form a band gap of $\sim 1.75 \text{ eV}$ but that from the edges are in much higher energy, concentrated at -0.33 eV , indicating that the edges are highly reactive to decrease the ribbon stability. In contrast, for the 1T-18-aWNR, the occupied electron states contributed by the edges shift downward below -2 eV while the unoccupied edge states are found to be located at around 1.7 eV above the Fermi level. This contrasting behavior suggests that the edge of 1T phase is more stable than that of the 2H phase. This electronic feature from the edges is independent of the ribbon width, as shown in figures 4(a) and (b) for the 14 aWNR. However, the electronic states from the ribbon interior markedly change upon decreasing the ribbon width, in particular for the 1T ribbons. Especially, a band gap is observed in the DOSs contributed by the interior of 1T-aWNR and it increases with decreasing ribbon width as well. As the 1T phase is originally metallic, the enhanced semi-conducting nature in a narrower 1T ribbon signifies that the 1T ribbon interior becomes less unfavorable with respect to the 2H lattice. A clear picture thus emerges here accounting for the switch of stability between the 1T and 2H ribbons, that is the enhanced edge stability and less unfavorable interior in the 1T ribbons. Examining the spatially resolved LDOS of the 2H- and 1T-zWNRs also reveals similar mechanism for their switch of stability (see figure S4).

The electronic band structures and the spatial distribution of charge density also support our above analyses. Figures 5(a) and (c) show that 2H-14 and 18-aWNRs are typical semiconductors with the direct band gaps of 0.53 and 0.52 eV , which is significantly smaller than that in perfect 2H WSe_2 since the edge atoms introduce new flat bands near the Fermi level that narrow the band gap. A close examination of edges reveals that edge W atoms have four covalent bonds instead of six covalent bonds in perfect lattice. The resultant dangling bonds at the edges are the origin of these flat bands. In the case of 1T-aWNRs, the flat bands shift away from the Fermi level, which can be understood from two aspects. First, the edge W atoms are more uniformly surrounded by S atoms, close to the bond configurations in the perfect lattice. Second, most of the edge W atoms in an aWNR are coordinated with S atoms and all the edge W atoms in a zWNR are coordinated with S atoms. As such, the edge dangling bonds in the 1T ribbons are largely passivated. This is further illustrated by the charge density distribution. The distribution of charge density corresponding to the edge states in the 2H-aWNRs is

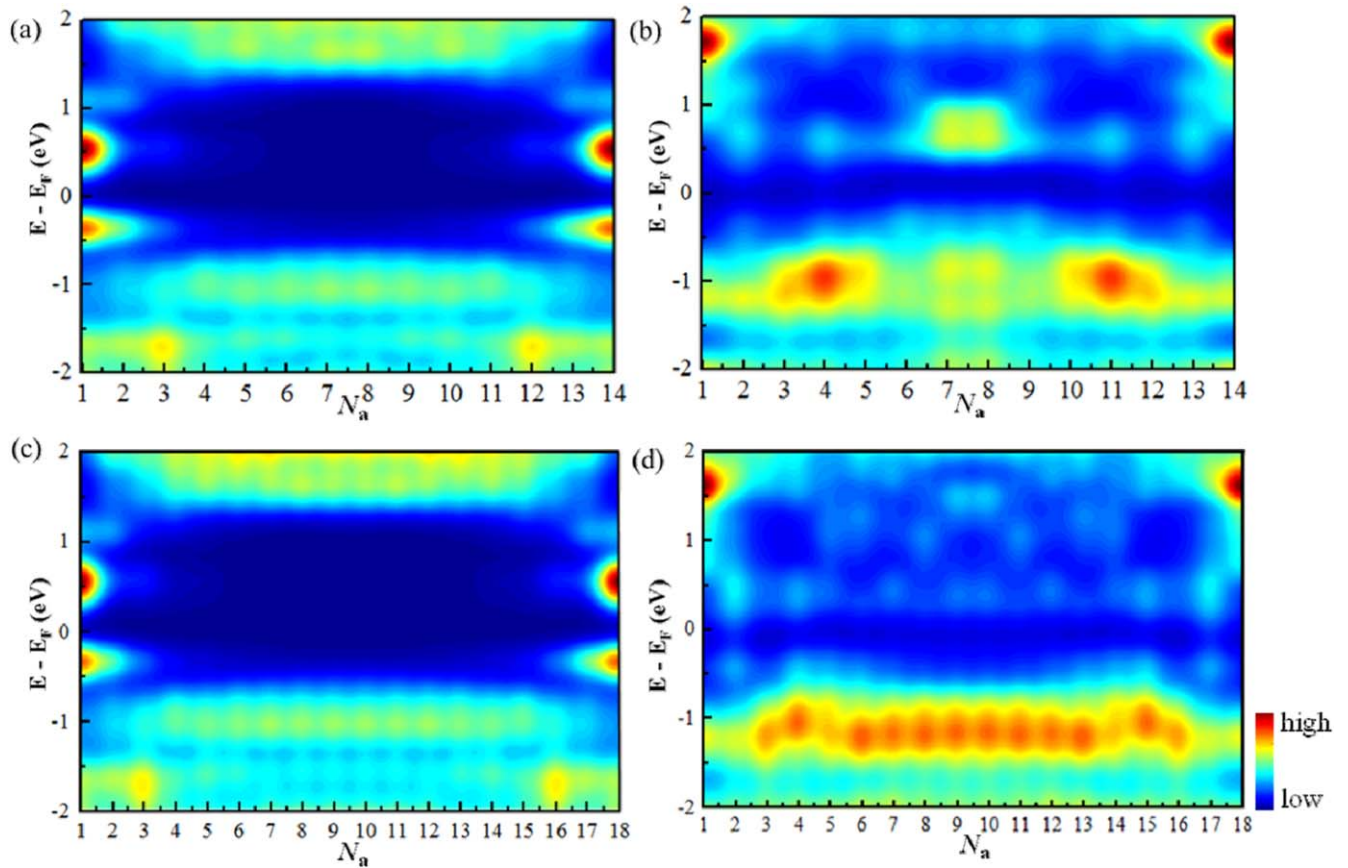


Figure 4. Spatially resolved local density of states of (a) 2H-14-aWNR, (b) 1T-14-aWNR, (c) 2H-18-aWNR and (d) 1T-18-aWNR.

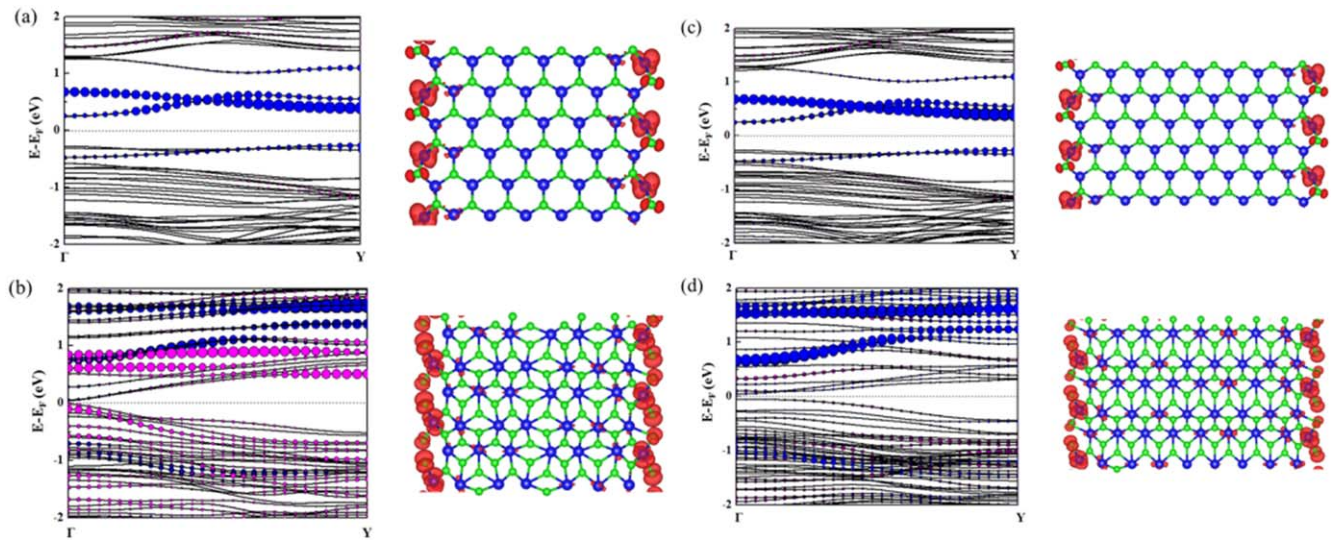


Figure 5. Electronic band structures and charge density of edge states of (a) 2H-14-aWNR, (b) 1T-14-aWNR, (c) 2H-18-aWNR and (d) 1T-18-aWNR. The bands projected to W 3d and S 3p orbitals from edge and center atoms are highlighted by blue and pink circles. The circle size reflects the weight of the orbital components in the bands.

found to be highly localized at the edges, while the counterpart in the 1T-aWNRs tends to extend along the edge and decay more clearly into the ribbon interior. The semi-conducting nature in the ribbon interior is also evident in the band structures of 1T-14 and 18-aWNRs. We can measure that the band gap of the ribbon interior increases with

decreasing size, from ~ 0.3 eV for 1T-18-aWNR to ~ 0.5 eV for 1T-14-aWNR. There are two possible reasons for the increased band gap. One is the quantum confinement effect and the other is the enhanced structural distortion in narrower 1T ribbon. An evidence for the latter is that the W atoms are apparently dimerized (like charge density wave [38]) not only

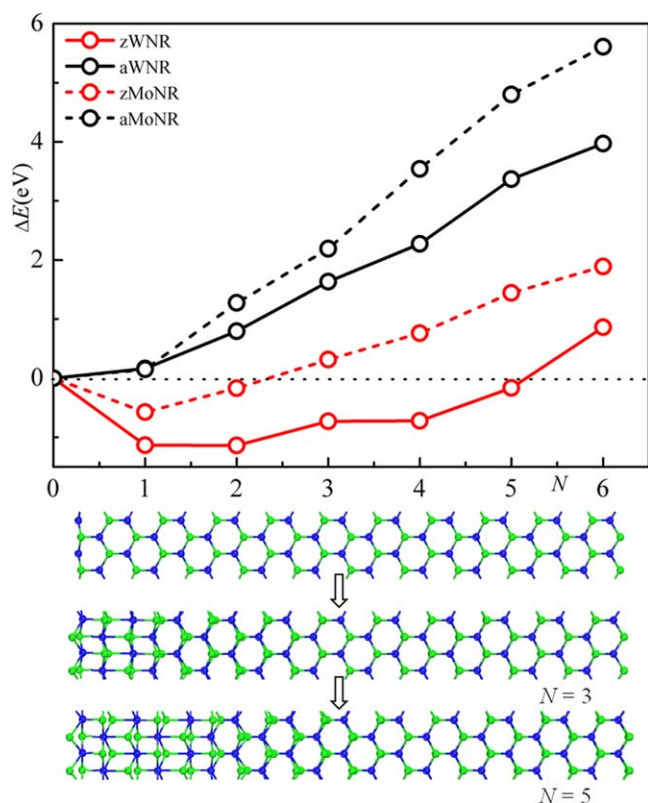


Figure 6. The energy differences between the transformed nanoribbons at each step of shifting atomic rows and the one in uniform 2H phase as a function of number of atomic rows. The insets at the bottom illustrate the atomic structures at $N = 0, 3$ and 5 for 21-zWNRs.

along the ribbon but also across the ribbon in the 14-aWNR, while such dimerization only appears along the ribbon in the 18-aWNR (see inserts in figures 5(b) and (d)). In addition, electronic band structures and charge density of edge states of 2H-6-zWNR, 1T-6-zWNR, 2H-10-zWNR and 1T-10-zWNR were shown in figure S5.

3.3. The process of phase transition

Our above results have revealed a phase crossover in MX_2 nanoribbon from thermodynamic point of view. To gain deeper insight into the phase transition, we examine possible processes of the transition from 2H to 1T nanoribbons, via a sequential step-by-step shift of atomic rows. Taking the 21-zWNRs and 41-aWNRs (with nearly identical width) as two prototype systems, we sequentially shift the atomic rows from the edge to that in the interior. The structure at each step of shifting is fully relaxed. The energy difference between the transformed nanoribbons at each step and the one in uniform 2H phase is shown as a function of step number N in figure 6. A positive energy difference suggests that the local lattice transition is energetically unfavorable.

Since both the 21-zWNR and 41-aWNR have large width, their corresponding 2H phase is more favorable than the 1T phase, as supported by figure 6. However, the two nanoribbons differ in the detailed process of transition. For zWNRs, this energy difference first decreases to a minimum

at $N = 2$ and then increases with the increasing N . This result suggests that the zWNR becomes more stable by locally adopting the 1T phase near the W edge, even though an energetically unfavorable interface is embedded in the ribbon. The local formation of 1T lattice in the 2H zWNR can be thermodynamically preferred until N increases to 5, as shown by the insets at the bottom of figure 6. The favorable coexistence of 1T and 2H phases in the 21-zWNR opens an interesting possibility of forming a metal-semiconducting heterostructure with atomic coherence across the interface. In contrast, for the aWNRs, the energy difference monotonically increases with the increasing N , suggesting that the local formation 1T lattice is not favored by energy in this case. The reason for this difference between zWNRs and aWNRs is likely due to the higher energy of 1T-2H interface in the aWNRs than that in the zWNRs. These results lead us to conclude that the aWNRs would prefer a uniform lattice and, as discussed, the 1T phase when they become narrow. Even for narrow aWNRs, sufficiently high temperature should be required to activate the phase transition in light of that the shift of atomic rows always costs energy in the aWNRs.

4. Conclusions

We have performed a comprehensive first-principles study of the ground state structure of MX_2 nanoribbons and their electronic structures. The MX_2 nanoribbons are shown to have a high level of phase tunability, from 2H phase favored by perfect 2D lattice to 1T phase with the decreasing ribbon width. The 1T phase is found to have increasingly lower energy than the 2H phase at a smaller ribbon width, and the critical ribbon width for favoring the 1T phase increases in MX_2 with heavier M, up to 2.50 nm for WSe_2 . The exceptional phase transition in nanoribbons is revealed to be originated from enhanced stability of the edges by the 1T bond configuration and an interesting electronic reconstruction of 1T lattice in the ribbon interior. Our results unravel a new fundamentally important aspect of low-dimensional MX_2 nanostructures and will promote further experimental and theoretical investigations in this direction.

Acknowledgments

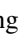
Computer resources were provided by XSEDE under allocation TG-DMR100029 and TG-DMR150091 and the DAVinCI cluster. This work was supported by National Natural Science Foundation of China (21720102006 to S-D Li, 21803037 to W-Y Zan, 11772153 to Z Z). The work at Rice was supported by the US Department of Energy (DE-SC0012547) and by the R. Welch Foundation (C-1590).

Conflicts of interest

There are no conflicts to declare.

ORCID iDs

Wenyan Zan  <https://orcid.org/0000-0001-6010-1848>

Zhuhua Zhang  <https://orcid.org/0000-0001-6406-0959>

Yang Yang  <https://orcid.org/0000-0003-3389-0268>

References

- [1] Chhowalla M, Shin H S, Eda G, Li L J, Loh K P and Zhang H 2013 The chemistry of two-dimensional layered transition metal dichalcogenide nanosheets *Nat. Chem.* **5** 263–75
- [2] Wang Q H, Kalantar-Zadeh K, Kis A, Coleman J N and Strano M S 2012 Electronics and optoelectronics of two-dimensional transition metal dichalcogenides *Nat. Nanotechnol.* **7** 699–712
- [3] Zhang Z H, Zou X L, Crespi V H and Yakobson B I 2013 Intrinsic magnetism of grain boundaries in two-dimensional metal dichalcogenides *ACS Nano* **7** 10475–81
- [4] Liu X F, Pan D X, Hong Y Z and Guo W L 2014 Bending poisson effect in two-dimensional crystals *Phys. Rev. Lett.* **112** 205502
- [5] Lu N, Guo H Y, Li L, Dai J, Wang L, Mei W N, Wu X J and Zeng X C 2014 MoS₂/MX₂ heterobilayers: bandgap engineering via tensile strain or external electrical field *Nanoscale* **6** 2879–86
- [6] Zan W, Geng W, Liu H and Yao X 2016 Electric-field and strain-tunable electronic properties of MoS₂/h-BN/graphene vertical heterostructures *Phys. Chem. Chem. Phys.* **18** 3159–64
- [7] Zan W Y, Geng W, Liu H X and Yao X J 2015 Influence of interface structures on the properties of molybdenum disulfide/graphene composites: a density functional theory study *J. Alloy Compd.* **649** 961–7
- [8] Zan W Y, Hu Z L, Zhang Z H and Yakobson B I 2016 Phase crossover in transition metal dichalcogenide nanoclusters *Nanoscale* **8** 19154–60
- [9] Lin Y C, Dumcenccon D O, Huang Y S and Suenaga K 2014 Atomic mechanism of the semiconducting-to-metallic phase transition in single-layered MoS₂ *Nat. Nanotechnol.* **9** 391–6
- [10] Kan M, Wang J Y, Li X W, Zhang S H, Li Y W, Kawazoe Y, Sun Q and Jena P 2014 Structures and phase transition of a MoS₂ monolayer *J. Phys. Chem. C* **118** 1515–22
- [11] Zhu J Q et al 2017 Argon plasma induced phase transition in monolayer MoS₂ *J. Am. Chem. Soc.* **139** 10216–9
- [12] Pandey M, Bothra P and Pati S K 2016 Phase transition of MoS₂ bilayer structures *J. Phys. Chem. C* **120** 3776–80
- [13] Kretschmer S, Komsa H P, Boggild P and Krashenninnikov A V 2017 Structural transformations in two-dimensional transition-metal dichalcogenide MoS₂ under an electron beam: insights from first-principles calculations *J. Phys. Chem. Lett.* **8** 3061–7
- [14] Duerloo K A N, Li Y and Reed E J 2014 Structural phase transitions in two-dimensional Mo- and W-dichalcogenide monolayers *Nat. Commun.* **5** 4214
- [15] Cho S et al 2015 Phase patterning for ohmic homojunction contact in MoTe₂ *Science* **349** 625–8
- [16] Voiry D, Mohite A and Chhowalla M 2015 Phase engineering of transition metal dichalcogenides *Chem. Soc. Rev.* **44** 2702–12
- [17] Sun X L, Wang Z G, Li Z J and Fu Y Q 2016 Origin of structural transformation in mono- and bi-layered molybdenum disulfide *Sci. Rep.* **6** 26666
- [18] Alyoruk M M, Aierken Y, Cakir D, Peeters F M and Sevik C 2015 Promising piezoelectric performance of single layer transition-metal dichalcogenides and dioxides *J. Phys. Chem. C* **119** 23231–7
- [19] Yu J H, Lee H R, Hong S S, Kong D S, Lee H W, Wang H T, Xiong F, Wang S and Cui Y 2015 Vertical heterostructure of two-dimensional MoS₂ and WSe₂ with vertically aligned layers *Nano Lett.* **15** 1031–5
- [20] Li B et al 2016 Solid-vapor reaction growth of transition-metal dichalcogenide monolayers *Angew. Chem. Int. Ed.* **55** 10656–61
- [21] Zan W Y, Geng W, Liu H X and Yao X J 2016 Field emission properties of two-dimensional VS₂-ZnO composites: a density functional theory study *J. Alloy Compd.* **658** 152–6
- [22] Yu H, Kutana A and Yakobson B I 2016 Carrier delocalization in two-dimensional coplanar p–n junctions of graphene and metal dichalcogenides *Nano Lett.* **16** 5032–6
- [23] Xu H et al 2016 Oscillating edge states in one-dimensional MoS₂ nanowires *Nat. Commun.* **7** 12904
- [24] Chen Y X, Cui P, Ren X B A, Zhang C D, Jin C H, Zhang Z Y and Shih C K 2017 Fabrication of MoSe₂ nanoribbons via an unusual morphological phase transition *Nat. Commun.* **8** 15135
- [25] Qi R F, Wang S L, Wang M X, Liu W T, Yan Z H, Bi X F and Huang Q S 2017 Towards well-defined MoS₂ nanoribbons on a large scale *Chem. Commun.* **53** 9757–60
- [26] Pan H and Zhang Y W 2012 Tuning the electronic and magnetic properties of MoS₂ nanoribbons by strain engineering *J. Phys. Chem. C* **116** 11752–7
- [27] Li Y F, Zhou Z, Zhang S B and Chen Z F 2008 MoS₂ nanoribbons: high stability and unusual electronic and magnetic properties *J. Am. Chem. Soc.* **130** 16739–44
- [28] Ataca C, Sahin H, Akturk E and Ciraci S 2011 Mechanical and electronic properties of MoS₂ nanoribbons and their defects *J. Phys. Chem. C* **115** 3934–41
- [29] Esfahani D N, Leenaerts O, Sahin H, Partoens B and Peeters F M 2015 Structural transitions in monolayer MoS₂ by lithium adsorption *J. Phys. Chem. C* **119** 10602–9
- [30] He H, Lu P F, Wu L Y, Zhang C F, Song Y X, Guan P F and Wang S M 2016 Structural properties and phase transition of Na adsorption on monolayer MoS₂ *Nanoscale Res. Lett.* **11** 330
- [31] Zhou Y and Reed E J 2015 Structural phase stability control of monolayer MoTe₂ with adsorbed atoms and molecules *J. Phys. Chem. C* **119** 21674–80
- [32] Kan M, Wang B, Lee Y H and Sun Q 2015 A density functional theory study of the tunable structure, magnetism and metal-insulator phase transition in VS₂ monolayers induced by in-plane biaxial strain *Nano Res.* **8** 1348–56
- [33] Zhang C X et al 2016 Charge mediated reversible metal-insulator transition in monolayer MoTe₂ and W_xMo_{1–x}Te₂ alloy *ACS Nano* **10** 7370–5
- [34] Zhou W, Zou X L, Najmaei S, Liu Z, Shi Y M, Kong J, Lou J, Ajayan P M, Yakobson B I and Idrobo J C 2013 Intrinsic structural defects in monolayer molybdenum disulfide *Nano Lett.* **13** 2615–22
- [35] Kresse G and Furthmüller J 1996 Efficient iterative schemes for *ab initio* total-energy calculations using a plane-wave basis set *Phys. Rev. B* **54** 11169–86
- [36] Kresse G and Joubert D 1999 From ultrasoft pseudopotentials to the projector augmented-wave method *Phys. Rev. B* **59** 1758–75
- [37] Perdew J P and Wang Y 1992 Accurate and simple analytic representation of the electron-gas correlation-energy *Phys. Rev. B* **45** 13244–9
- [38] Mcmillan W L 1976 Theory of discommensurations and the commensurate-incommensurate charge-density-wave phase transition *Phys. Rev. B* **14** 1496–502